Paracrystalline microdomains in monatomic liquids. I. Radial density functions of liquid lead at 350, 450, and 550°C

B. Steffen

Teilinstitut für Strukturforschung am Fritz-Haber-Institut der Max-Planck-Gesellschaft, Berlin-Dahlem, Germany

(Received 14 May 1975)

An alignment procedure for ϑ-ϑ-goniometers was developed, using a NaCl single crystal floating on mercury. This method also allows the determination of the wavelength acceptance curve of the monochromator and thereby the elimination of the incoherent Compton scattering. The structure factors of liquid lead at 350, 450, and 550°C were determined with a commercial x-ray diffractometer using Mo $K\alpha$ radiation. The resultant radial density functions were compared to those of Kaplow *et al.* and North *et al.* and found to lie at most distances between their results.

I. INTRODUCTION

The interference functions of molten metals generally show only a few more or less diffuse maxima. Recently it has nevertheless become more and more apparent that very exact measurements of the liquid-structure factor are necessary in order to evaluate the resultant radial density functions in a way which gives three-dimensional-structure data of the melt (this method of analysis will soon be published).

The radial density functions of liquid lead at different temperatures have been determined from x-ray measurements by Kaplow *et al.*[1] and from neutron measurements by North *et al.*[2] Since there are still some differences between their results, it seemed worthwhile to repeat the x-ray measurements. For this purpose a commercial diffractometer called GSD (gravitation symmetrical diffractometer) from Seifert and Co., Hamburg, was used. The essential features of the diffractometer are shown in Fig. 1.

The sample is positioned horizontally while the x-ray tube and the detecting system are moved synchronously in a circle determined by the Bragg-Brentano focusing conditions. A bent-quartz monochromator is placed behind the specimen in order to remove the fluorescence radiation and the Compton modified scattering at high scattering angles. The intensity is recorded by a NaI(Tl) Berthold scintillation counter with a energy resolution of about 50%. The resulting pulses are discriminated electronically. Since the goniometer is built on three adjustable legs, its orientation with respect to the sample surface can easily be adjusted. When looking for goniometer alignment methods in the literature one finds either nothing or little information.[3,4]

One of the most important things to consider while measuring liquid-structure factors is the alignment of the primary beam so that it hits the center of the goniometer. The method described below has the advantage that the alignment can be performed directly with the help of the x-ray system which is used for the measurements and without any special optical or mechanical adjustment devices such as a microscope, fluorescent screens, or needles. Another advantage is that the single crystal which is used for adjustment can also be used to determine the wavelength acceptance curve of the monochromator.

II. ALIGNMENT

After a thorough horizontal adjustment of the diffractometer (without monochromator) the receiving slit on the detector arm is shifted until the primary beam is symmetric about the $\vartheta = 0°$ position. Next the crucible is filled with mercury upon which a plane-parallel NaCl single crystal with (100) orientation is laid. This guarantees a horizontal orientation of the (100) net planes. The goniometer is then brought into the theoretical position of the NaCl 200 reflection. The heights of the three goniometer legs are then varied until maximum intensity is reached. In this way the goniometer will be aligned horizontally. There is, however, still the possibility that the primary beam will not pass through the center of the goniometer as shown in Fig. 2.

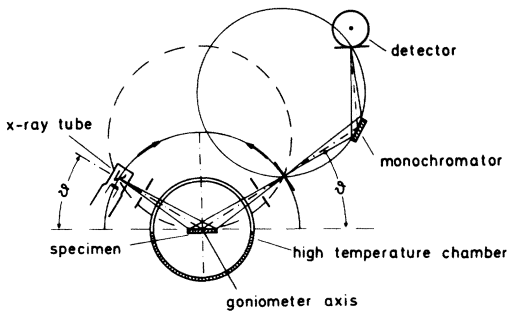

FIG. 1. Schematic drawing of the Seifert ϑ-ϑ goniometer.

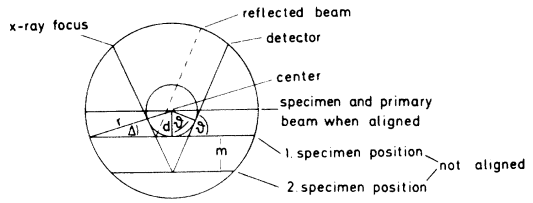

FIG. 2. Schematic drawing of the procedure of the adjustment of the goniometer.

In order to find the angle Δ by which the $\vartheta = 0°$ position is in error, we change in that angle-position the height of the goniometer until the crystal surface is in the middle of the primary beam (intensity is now one-half of the value without the crystal). This height is designated as position 1 in Fig. 2. The height of the crystal is now changed for each $h00$ reflection until maximum intensity is reached. That could occur, for example, at position 2 in Fig. 2, where the sample height is changed by m compared to position 1. Assuming that the primary beam passes the goniometer center at a distance d and that ϑ is the theoretical $h00$ reflection angle we get for the height m by which the crystal has to be shifted

$$m = r \sin\Delta\,(1/\cos\vartheta - 1) \ ,$$

which follows directly from

$$\cos\vartheta = d/(d+m) \quad \text{and} \quad d = r\sin\Delta \ . \tag{1}$$

The radius of the goniometer circle r here is 250 mm. If we draw the sample-height change m as a function of

$$1/\cos\vartheta - 1 \tag{2}$$

for a few $h00$ reflection angles ϑ, we get from the slope of the resulting line the angle Δ by which the $\vartheta = 0°$ position has to be changed. In that new $\vartheta = 0°$ position the divergence slit at the x-ray tube is shifted until the primary beam without the crystal is again symmetric about the new $\vartheta = 0°$ position. Now the entire procedure can be repeated in order to check the alignment.

The comparison of the measured and the theoretical Bragg angles for the NaCl 100 reflections finally gave deviations of less than 1%. This is thus at least the accuracy with which the angular data of the liquid-structure factor can be measured.

III. COMPTON CORRECTION

In order to find which part of the Compton-scattered intensity will finally reach the detector, one has to know the wavelength acceptance curve of the monochromator. This can easily be measured with the help of the single crystal still floating on the mercury. Before the monochromator is replaced, the NaCl 400 reflection is used to measure at a tube voltage of 20 kV the wavelength distribution I_0 of the x-ray tube (Fig. 3). The monochromator then is replaced and adjusted, and the same measurement is repeated. The resulting curve I_{Mo} is also shown in Fig. 3, as a function of the wavelength λ which can be calculated from the measured reflection angle ϑ by Bragg's equation,

$$\lambda = (\sin\vartheta/\sin\vartheta_0)\,\lambda_0 \ , \tag{3}$$

where $\vartheta_0 = 14.57°$ is the 400 reflection angle for Mo $K\alpha_1$ radiation with $\lambda_0 = 0.7094$ Å. A voltage of 20 kV was chosen because this is the excitation voltage of the Mo K_α radiation. With a higher voltage one would get a mixture of the wavelengths coming from different $h00$ reflections plus diffuse scattering of the Mo K_α peak. At the left-hand side of Fig. 3, for instance, one can see the long-wavelength part of the 200 reflection. It does not disturb our 400 spectrum in the region of interest, using the 20-kV voltage. The λ_{min} value of the white spectrum at 20 kV is 0.62 Å, which agrees fairly well with the left-hand tail of the I_0 curve. From this one recognizes that the white spectrum of the 600 reflection also does not disturb the spectrum reflected by the 400, because its left-hand tail of λ_{min} lies at $0.62 \times \frac{3}{2}$ Å.

By division of the two functions in Fig. 3, we get the wavelength acceptance curve of the monochromator, which is shown in Fig. 4. It has an asymmetry at longer wavelengths which is caused by the wavelength-dependent penetration depth of the x rays, an effect that has been described by Scott.[5] The maximum of the line profile of the Compton-scattered intensity has wavelength

$$\lambda = \lambda_0 + 2\,\lambda_c \sin^2\vartheta \ , \tag{4}$$

where λ_0 is the wavelength of the incident radiation, $\lambda_c = 0.0243$ Å is the Compton wavelength of an

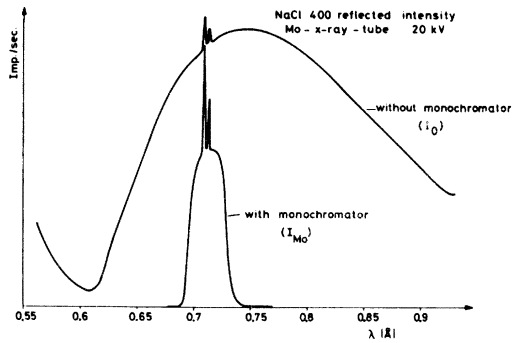

FIG. 3. Wavelength dependence of the white spectrum of the Mo x-ray tube at 20 kV (I_0) and the intensity distribution (I_{Mo}) behind the monochromator (enlarged five-fold).

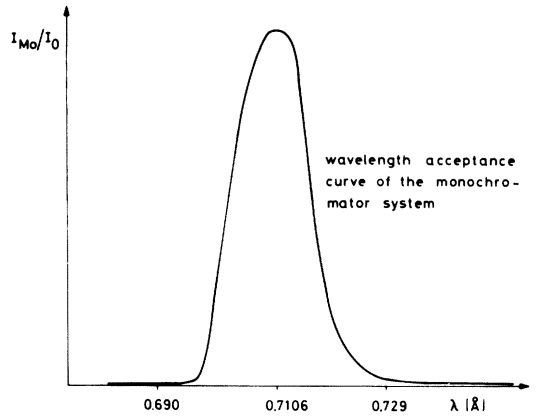

FIG. 4. Acceptance curve of the monochromator.

electron, and ϑ is the half-scattering angle.

The relativistically corrected Compton intensity $I_{Compton}$ is shown in Fig. 5 according to Sagel[6] as a function of

$$s = 4\pi \sin\vartheta/\lambda \quad . \tag{5}$$

If multiplied by I_{Mo}/I_0 it gives the Compton scattering I' reflected by the monochromator. This incoherent scattered intensity is everywhere less than 1% of the coherent-scattered intensity, in the case of liquid lead.

It should be mentioned that for light elements the Compton-scattered intensity becomes comparable with the coherent-scattered intensity. One then must take into account the fact that $I_{Compton}$ has a spectrum for each s value and that the primary radiation has a spectrum too. Many curves of the type $I'(s)$ of Fig. 5 must then be superimposed. In our case the influence of Compton scattering is negligible.

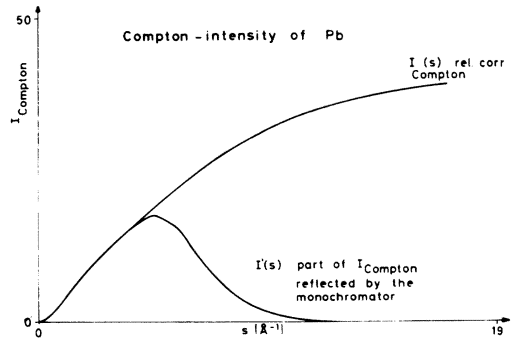

FIG. 5. Theoretical relativistic Compton intensity $I_{Compton}$ and its contribution behind the monochromator.

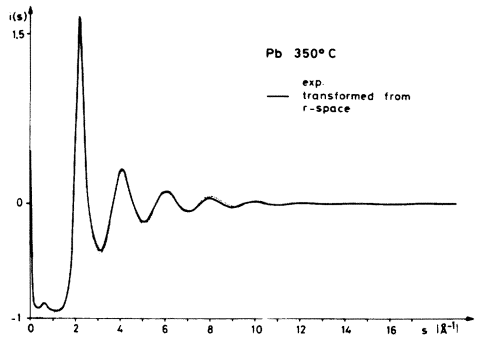

FIG. 6. Corrected intensity $i(s)$. Dotted line, directly measured; solid line, Fourier transform of the radial density distribution.

IV. INTENSITY FUNCTION OF LEAD

The coherent-scattered intensities of lead at 350 and 450 °C were each measured three times. The atmosphere was pure H_2. The 550 °C measurement was done twice within an atmosphere of 90% He and 10% H_2. During measurements the surface of the sample remained clean and mirror-like. The statistical error of the final intensity values was about 1%. Since measurements could be taken only for $s \geq s_{min} = 1.2$ Å^{-1}, the missing intensity values were extrapolated parabolically to $s = 0$ Å^{-1}. An evaluation of the intensity curve $I(s)$ for $s \geq s_{max} = 12.5$ Å^{-1} was impossible because in this case the statistical error became greater than the modulation of the intensity curve.

After polarization correction the normalizing factor F can, according to Hosemann and Schoknecht,[7] be determined from

$$F\int_0^{s_{max}} s^2 I(s)\,ds = \int_0^{s_{max}} s^2 f^2(s)\,ds \quad , \tag{6}$$

where $I(s)$ is the corrected intensity and $f^2(s)$ is

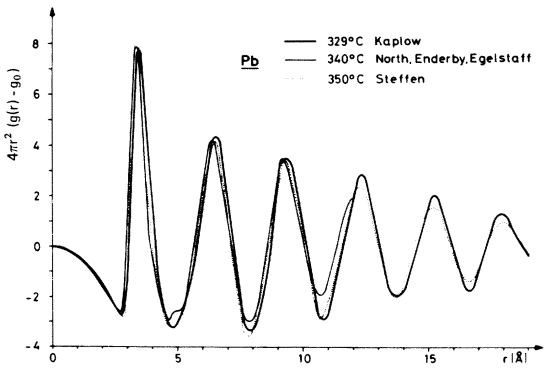

FIG. 7. Radial density function of lead at 350 °C compared with the results of Kaplow *et al.* (Ref. 1) and North *et al.* (Ref. 2).

TABLE I. Experimental intensity function $i(s)$ at three temperatures T_n.

s (Å^{-1})	350 °C	450 °C	550 °C
1.2	−0.938	−0.925	−0.918
1.3	−0.925	−0.910	−0.903
1.4	−0.911	−0.894	−0.882
1.5	−0.832	−0.857	−0.835
1.6	−0.833	−0.800	−0.771
1.7	−0.752	−0.702	−0.664
1.8	−0.580	−0.505	−0.467
1.9	−0.275	−0.164	−0.109
2.0	0.346	0.452	0.426
2.1	1.322	1.204	1.005
2.2	1.656	1.481	1.266
2.3	1.175	1.061	1.016
2.4	0.536	0.539	0.503
2.5	0.170	0.178	0.192
2.6	−0.047	0.006	−0.005
2.7	−0.187	−0.141	−0.133
2.8	−0.296	−0.244	−0.210
2.9	−0.359	−0.312	−0.293
3.0	−0.409	−0.375	−0.358
3.1	−0.438	−0.389	−0.380
3.2	−0.425	−0.386	−0.360
3.3	−0.378	−0.356	−0.326
3.4	−0.328	−0.285	−0.276
3.5	−0.235	−0.204	−0.204
3.6	−0.109	−0.104	−0.111
3.7	−0.004	0.010	0.000
3.8	0.114	0.114	0.080
3.9	0.211	0.206	0.180
4.0	0.264	0.259	0.230
4.1	0.294	0.278	0.245
4.2	0.266	0.277	0.243
4.3	0.219	0.227	0.210
4.4	0.141	0.175	0.148
4.5	0.069	0.089	0.082
4.6	−0.001	0.033	0.037
4.7	−0.082	−0.025	−0.012
4.8	−0.112	−0.087	−0.073
4.9	−0.160	−0.115	−0.106
5.0	−0.172	−0.123	−0.129
5.1	−0.189	−0.143	−0.132
5.2	−0.160	−0.133	−0.124
5.3	−0.140	−0.097	−0.102
5.4	−0.105	−0.082	−0.074
5.5	−0.043	−0.039	−0.037
5.6	0.005	0.000	−0.003
5.7	0.034	0.038	0.025
5.8	0.087	0.085	0.059
5.9	0.106	0.112	0.081
6.0	0.106	0.129	0.093
6.1	0.115	0.104	0.099
6.2	0.103	0.107	0.097
6.3	0.082	0.094	0.087
6.4	0.063	0.072	0.072
6.5	0.027	0.057	0.054
6.6	−0.018	0.022	0.029
6.7	−0.005	0.000	0.009
6.8	−0.038	−0.025	−0.007

TABLE I. (*Continued*).

s (Å^{-1})	350 °C	450 °C	550 °C
6.9	−0.058	−0.023	−0.028
7.0	−0.052	−0.036	−0.039
7.1	−0.059	−0.043	−0.042
7.2	−0.051	−0.034	−0.042
7.3	−0.047	−0.026	−0.036
7.4	−0.025	−0.022	−0.024
7.5	0.002	−0.005	−0.007
7.6	0.027	0.008	0.009
7.7	0.047	0.229	0.026
7.8	0.063	0.043	0.041
7.9	0.053	0.043	0.049
8.0	0.067	0.062	0.052
8.1	0.084	0.048	0.049
8.2	0.076	0.047	0.048
8.3	0.054	0.061	0.043
8.4	0.030	0.016	0.041
8.5	0.038	0.026	0.038
8.6	0.024	0.039	0.032
8.7	0.008	0.009	0.023
8.8	−0.007	−0.016	0.013
8.9	−0.010	−0.006	0.000
9.0	−0.004	−0.011	−0.008
9.1	−0.009	−0.022	−0.010
9.2	−0.026	−0.014	−0.013
9.3	−0.016	−0.026	−0.016
9.4	−0.004	−0.016	−0.016
9.5	0.002	−0.002	−0.016
9.6	0.009	0.006	−0.012
9.7	0.025	0.005	−0.008
9.8	0.011	0.009	0.000
9.9	0.021	0.010	0.005
10.0	0.034	0.089	0.011
10.1	0.042	0.005	0.018
10.2	0.026	0.008	0.021
10.3	0.025	0.009	0.025
10.4	0.027	0.021	0.025
10.5	−0.016	0.000	0.025
10.6	−0.004	−0.023	0.025
10.7	−0.025	−0.025	0.025
10.8	−0.010	−0.012	0.024
10.9	0.002	−0.005	0.023
11.0	0.001	−0.014	0.020
11.1	−0.015	−0.016	0.009
11.2	−0.015	−0.013	0.003
11.3	−0.004	−0.019	0.000
11.4	−0.010	0.084	0.000
11.5	−0.001	0.001	−0.003
11.6	0.002	−0.017	−0.006
11.7	0.008	−0.021	−0.007
11.8	−0.001	−0.025	−0.010
11.9	0.010	−0.016	−0.010
12.0	0.013	−0.016	−0.009
12.1	0.014	−0.009	−0.008
12.2	−0.005	−0.019	−0.007
12.3	0.001	−0.013	−0.005
12.4	−0.001	−0.205	−0.004
12.5	0.003	−0.004	−0.001

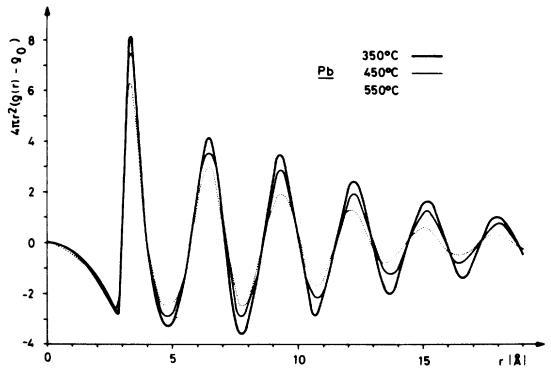

FIG. 8. Radial density function of lead at 350, 450, and 550 °C.

the atomic scattering factor. In this work $f^2(s)$ was taken from Cromer and Mann,[8] with the dispersion correction given by Dauben and Templeton.[9] Strictly speaking $I(s)$ does not contain the reflection 000, contrary to $f^2(s)$ which expands over the entire Fourier space. Its contribution is negligible (smaller than 0.5%) compared with the integral intensities of all other interference terms. It becomes much smaller if integration is carried out beginning at $s_{min} > 0$.

V. RADIAL DENSITY DISTRIBUTION OF LEAD

By Fourier transformation of

$$i(s) = FI(s)/f^2(s) - 1 \quad , \tag{7}$$

we get, according to Zernike and Prins,[10] the so-called radial density function $\rho(r)$

$$4\pi r^2 [\rho(r) - \rho_0] = \frac{2r}{\pi} \int_0^\infty si(s) \sin(rs)\, ds \quad , \tag{8}$$

where ρ_0 is the mean number density of the centers of the Pb atoms and r is the distance from an atom at the origin. Since the integration in reality cannot be carried out to infinity, the resulting radial density function is disturbed by the so-called termination effect which produces more or less weak secondary maxima with a wavelength of about $2\pi/s_{max}$ (Å) (see Hosemann *et al.*[11]). After removing these ripples by hand the curves were transformed back and compared with the measured intensity values in order to see whether serious faults had arisen by this smoothing of the radial density functions.

Figure 6 shows as an example the measured intensity of lead at 350 °C compared with the inverse Fourier-transform of the smoothened density function. Both agree very well for $s \geq 1$ Å^{-1}. The increasing values of the inverse-transformed intensity at small s are due to small errors in the smoothened density function at large r and play no role, since here the intensity could not be measured and because the one-dimensional backtransform is given by $si(s)$. The division by s gives naturally a strong amplification of little faults at small s.

Figure 7 shows the comparison of our radial density function with those of Kaplow *et al.*[1] and North *et al.*[2] As can be seen, our curve, at most distances, lies between the other two. This fact can be considered as a confirmation of the satisfying alignment method described above.

A quantitative analysis of the remaining differences between the x-ray data and the neutron data of North *et al.* was not possible because we were not able to get tabulated values of the neutron data. We had to take the values from the pictures in their publication, which is good enough for qualitative but not for quantitative considerations. In order to avoid such difficulties for others, our measured structure factors are given in Table I. A comparison of the radial density functions at three temperatures is shown in Fig. 8.

The only temperature effect that the radial density functions show is an increasing damping. The positions of the maxima and minima remain unchanged. Only the position of the first maximum seems to be shifted somewhat to smaller distance with increasing temperature. There is also an increase in the asymmetry of the first maximum. Although the temperature effects are small, one nevertheless can deduce some interesting information, as will be discussed in a subsequent paper.

ACKNOWLEDGMENT

The author is very grateful to the Deutsche Forschungsgemeinschaft, which supported this work.

[1] R. Kaplow, S. L. Strong, and B. L. Averbach, Phys. Rev. 5, A138 (1965).
[2] D. M. North, J. E. Enderby, and P. A. Egelstaff, J. Phys. Chem. 2, 1 (1968).
[3] H. Ruppersberg, Mem. Sci. Rev. Met. 61, 709 (1964).
[4] C. N. J. Wagner, H. Ocken, and M. L. Joshi, Z. Naturforsch. A 20, 325 (1964).
[5] R. E. Scott, Rev. Sci. Instrum. 35, 118 (1964).
[6] K. Sagel, *Tabellen zur Röntgenstrukturanalyse* (Springer, Berlin, 1958).
[7] R. Hosemann, and G. Schoknecht, Z. Naturforsch. A 12, 932 (1957).
[8] D. T. Cromer and J. B. Mann, Acta Crystallogr. A 24, 312 (1968).
[9] C. H. Dauben and D. H. Templeton, Acta Crystallogr. 8, 841 (1955).
[10] F. Zernike and J. A. Prins, Z. Phys. 41, 184 (1927).
[11] R. Hosemann, K. Lemm, and H. Krebs, Z. Phys. Chem. 41, 314 (1964).